

This document is the unedited Author's version of a Submitted Work that was subsequently accepted for publication in [JournalTitle], copyright © American Chemical Society after peer review. To access the final edited and published work see [insert ACS Articles on Request author-directed link to Published Work, see <http://pubs.acs.org/page/policy/articlesonrequest/index.html>].

## **Self-assembling ELR-based nanoparticles as smart drug-delivery systems modulating cellular growth via Akt**

Juan Gonzalez-Valdivieso<sup>1</sup>, Alessandra Girotti<sup>1</sup>, Raquel Muñoz<sup>1</sup>, J. Carlos Rodriguez-Cabello<sup>1</sup> and F. Javier Arias<sup>1\*</sup>.

<sup>1</sup>BIOFORGE (Group for Advanced Materials and Nanobiotechnology), CIBER-BBN, University of Valladolid, 47011 Valladolid, Spain.

\*Corresponding author: [arias@bioforge.uva.es](mailto:arias@bioforge.uva.es)

### **Abstract**

This work investigates the physicochemical properties and *in vitro* accuracy of a genetically engineered drug delivery system based on elastin-like block recombinamers. The DNA recombinant technics allowed us to create this smart complex polymer containing bioactive sequences for internalization, lysosome activation under acidic pH and blockage of cellular growth by a small peptide inhibitor. The recombinant polymer reversibly self-assembled, when temperature was increased above 15°C, into nanoparticles with a diameter of 72 nm and negative surface charge. Furthermore, smart nanoparticles were showed to enter in the cells via clathrin-dependent endocytosis, and properly blocked phosphorylation and consequent activation of Akt kinase. This system provoked apoptosis-mediated cell death in breast and colorectal cancer cells, which possess higher expression levels of Akt, whereas non-cancerous cells, such as endothelial cells, fibroblasts and mesenchymal stem cells, were

not affected. Hence, we conclude that the conformational complexity of this smart elastin-like recombinamer leads to achieve successful drug delivery in targeted cells and could be a promising approach as nanocarriers with bioactive peptides in order to modulate multiple cellular processes involved in different diseases.

**Keywords:** drug delivery, nanoparticles, elastin-like recombinamers (ELRs), Akt,

## **1. Introduction**

One of the limitations of modern medicine is the lack of efficient drug carriers. Such carriers should accomplish their main function, namely release of a drug in a targeted tissue, so as to achieve two benefits: an increase in drug efficacy and a reduction in possible adverse side effects.<sup>1</sup> The development of a good carrier for a specific drug is of particular importance as, in some cases, the therapeutic dose of a drug is so high that it cannot be used without causing severe damage to other organs.<sup>2</sup> One of the most recent therapeutic approaches is based on smart advanced biomaterials. New biomaterials are thought to be an interesting alternative for drug delivery,<sup>3-4</sup> as they are able to overcome the limitations of chemotherapy and improve the action of chemotherapeutic agents.<sup>5-6</sup> Multifunctional carriers have been proposed to overcome these deficiencies.<sup>7</sup> Although significant progress has been made in the field of synthetic devices with improved polymerization efficiency and lower polydispersities, genetically engineered polymers provide us the control to build advanced delivery carriers with acquired functionalities.<sup>8</sup>

Elastin-like recombinamers (ELRs) are one such biomaterial. ELRs are biopolymers based on short pentapeptide repeats found in the sequence of natural elastin, mainly the VPGXG pentapeptide, where X can be any amino acid except proline. The term ELR refers to those elastin-like polypeptides (ELPs) manufactured using genetic-engineering techniques.

Recombinant DNA technology allows us to design ELRs with full control over the amino acid sequence and include different functionalities and bioactive sequences.<sup>9-10</sup> As such, ELRs presenting characteristic features are a novel alternative for the development of new biomedical devices because of their biological and mechanical properties, such as biocompatibility, biodegradability, and thermally and environmentally responsive behaviour.<sup>11</sup> Moreover, ELRs have gained notable interest in the last years due to their lack of toxicity and immunogenicity as a consequence of their protein nature. ELRs exhibit an inverse temperature transition (ITT), which means that below a characteristic temperature, the so-called transition temperature ( $T_t$ ), they remain soluble in a random coil conformation, self-assembling hydrophobically above this  $T_t$  and resulting in the reversible formation of coacervates due to a conformational reorganization at the molecular level. Coacervation of the polymer backbone can be triggered by different factors, including temperature, pH, light, ion concentration, etc. In addition, their stimulus-responsive behaviour can be tuned as  $T_t$  is controlled by the amino-acid composition of the recombinamer.<sup>12</sup> Given their cell-friendly behaviour, tunable mechanical properties, thermal sensitivity, and ability to self-assemble, they are useful biomaterials for most applications in the fields of nanotechnology and biomedicine and, specifically, for controlled drug delivery.<sup>13-17</sup>

Cancer is one of the potential applications of drug delivery systems as it is one of the most common diseases worldwide. Indeed, according to the World Health Organization, 14.1 million new cases of cancer are reported each year, with around 8.2 million cancer-related deaths. As cancer is a very complex disease with multiple origins and evolution states, different approaches are needed to tackle this illness. Although different therapies have been developed for cancer treatment, chemotherapy suffers from numerous problems, such as cytotoxicity, poor tumour accumulation and dose-limiting side effects.<sup>18</sup> Consequently, new

therapeutic approaches are needed to improve the diagnosis at earlier stages and increase the rate of treatment success. Advanced drug delivery systems enable to control the release of drugs in a specific cell or tissue, so smart bioresponsive biomaterials able to self-assemble and act under certain stimuli emerge as promising approaches for the achievement of reduced doses of the drugs and limited side effects.

Due to the poor tumour accumulation of standard drugs used in chemotherapy, carriers have become an interesting approach for drug-delivery purposes.<sup>19</sup> Nanoparticle-based delivery can reduce side effects by redistributing drug accumulation away from critical organs, such as the kidney or liver, thus allowing the administration of larger doses than is possible with free drugs.<sup>20</sup> As tumours have a porous vasculature, aberrant vascular endothelium and enhanced vascular permeability, 10–100 nm sized nanoparticles accumulate in tumours because of the enhanced permeability and retention effect (EPR).<sup>21</sup> This effect arises due to the fact that tumours have no functional lymphatic vessels, thus resulting in inefficient drainage from tumour tissue.<sup>22-23</sup> As such, nanoparticles are able to enter into the interstitial space but are not efficiently removed,<sup>24</sup> thus being retained in the tumor tissue.

The choice of the specific target in drug delivery makes the difference between whether healthy tissues are affected or not.<sup>25</sup> In this regard, cancer markers, such as overexpressed receptors and cytoplasmic proteins, are the most widely used targeting systems due to their higher expression in cancerous cells when compared to non-cancerous cells.<sup>18, 22</sup> Consequently, novel strategies that target overexpressed proteins could be of interest when determining how to stop uncontrolled cell proliferation, which is markedly faster in cancerous cells. Of these proteins, Akt stands out due to its important activity in controlling multiple signalling pathways and processes in cells.<sup>26</sup> Akt is a protein kinase that plays a central role in the regulation of multiple cellular processes, enhancing cellular proliferation,

metabolism and motility and inhibiting apoptosis.<sup>26</sup> It has three differentiated functional regions, namely the N-terminal pleckstrin homology domain (PH), the central catalytic domain and, finally, the C-terminal hydrophobic region.<sup>27</sup> In response to growth factors, Akt is activated by products of phosphatidyl inositol triphosphate generated by PI3K. These lipid products bind to the PH domain of Akt, thereby inducing a conformational change and allowing PDK1 to phosphorylate threonine 308. Phosphorylation of serine 473 and membrane anchoring are also required after threonine 308 phosphorylation for final activation of Akt kinase.<sup>28</sup> There are three different isoforms (Akt1, Akt2 and Akt3) in mammalian cells. Akt1 is the most abundant isoform and is overexpressed in multiple types of cancer, such as colon, pancreatic, breast, ovarian and lung neoplastic diseases.<sup>29</sup> As such, Akt is an attractive target for drug design and development. In light of this, Hiromura *et al.* have developed a small peptide (Akt-in) that accurately prevents phosphatidyl inositol species from binding to the pleckstrin homology domain (PH) of Akt by causing conformational changes, thereby inhibiting membrane translocation and Akt activation. This inhibitor prevents Akt kinase activity and, consequently, a biological response downstream. Moreover, Akt-in inhibits both *in vitro* proliferation and anti-apoptosis action as well as *in vivo* tumor progression.<sup>30</sup>

The objectives of this study were to synthesize and characterize a smart stimulus-responsive therapeutic system that can be modulated for application in different cells depending. Only recombinant technology allows us to create multi-functional block copolymers that can self-assemble into versatile NPs carrying the peptidic inhibitor of Akt, in a targeted and protected manner, and are specifically released in the intracellular environment. In light of the above, we have developed ELR nanoparticles carrying the peptidic inhibitor of protein kinase Akt (Akt-in). Moreover, we have determined *in vitro* the therapeutic window in which tumor cells

are affected and normal ones not, and have studied their internalization pathway and intracellular trafficking.

## **2. Materials and methods**

### **2.1 Chemical reagents and cell lines**

Genes for LAEL, Cathepsin D sensitive peptide, H5 peptide and Akt-in were acquired from NZYTECH (Portugal). *Escherichia coli* BLR (DE3) strain was supplied by Novagen. Chloroquine, filipin, amiloride, and monodansylcadaverine were purchased from Sigma-Aldrich. Pepstatin A was acquired from Apollo Scientific. Primary antibodies against Akt (#9272),  $\rho$ -Akt Ser473 (#9271) and GAPDH (sc-32233) were purchased from Cell Signaling and Santa Cruz Biotechnology. Goat secondary antibodies against rabbit (ab6721) and mouse (ab205719) were supplied by Abcam. Cell lysis buffer and Bradford reagent were supplied by Sigma-Aldrich. Human adipose-derived mesenchymal stem cells (hMSCs, R7788-115), basal medium Dulbecco's Modified Eagle's Medium (DMEM), Minimum Essential Medium (MEM), Fetal Bovine Serum (FBS), penicillin streptomycin solution, trypsin-EDTA, DPBS, glutamine, non-essential amino acids (NEAA) and LIVE/DEAD® Viability/Cytotoxicity Kit for mammalian cells were supplied by Invitrogen (USA). Human umbilical vein endothelial cells (HUVEC cc-2517), medium 200, low serum growth supplement (LSGS), L-15 medium and gentamicin/amphotericin solution were purchased from Gibco. Human foreskin fibroblasts (HFF-1, SCRC-1041) were purchased from the American Type Culture Collection (ATCC, USA). Human breast cancer (MCF-7, 86012803 ECACC) and human colorectal cancer (Caco-2, 86010202 ECACC) cell lines were supplied by Sigma-Aldrich.

### **2.2 ELR design, bioproduction and purification**

The elastin-like recombinamers (ELR) used in this work were obtained as described elsewhere.<sup>31</sup> The final fusion genes with a fully controlled composition and chain length were constructed by sequential introduction of the monomer gene segments in a stepwise manner using the recursive directional ligation method (RDL). The DNA sequence of every cloning step was corroborated by DNA sequencing. Expression vectors containing the selected ELR genes were transformed into *Escherichia coli* BLR (DE3) strain (Novagen) for production. The ELR was then bioproduced in *Escherichia coli* in a 15-L bioreactor (Applikon Biotechnology, Netherlands) and purified by several cooling and heating purification cycles (inverse transition cycling) following centrifugation, taking advantage of the ability of these recombinamers to aggregate above their transition temperature. Endotoxins were removed from the ELR by way of additional NaCl and NaOH treatments.<sup>32</sup> Finally, the polymer was dialyzed against ultrapure water type I and sterilized by filtration (0.22  $\mu\text{m}$  filters Nalgene), and freeze-dried prior to storage. The molecular weight and purity of the recombinamers were determined by sodium dodecyl sulfate polyacrylamide gel electrophoresis (SDS-PAGE) and mass spectrometry (MALDI-TOF/MS), respectively. The amino acid composition was further verified by high performance liquid chromatography (HPLC) and nuclear magnetic resonance (NMR) spectroscopy by the Instrumental Techniques Laboratory of the University of Valladolid. Endotoxin levels were measured using the Endosafe-PTSTM test (Charles River, USA).

### **2.3 Differential Scanning Calorimetry (DSC)**

DSC experiments were performed using a Mettler Toledo 822e with liquid-nitrogen cooler. Both temperature and enthalpy were calibrated against an indium standard. Solutions were prepared by dissolving the ELRs in PBS (pH 7.4) at 50 mg/mL. A 20  $\mu\text{L}$  aliquot of each

solution and its corresponding PBS reference were subjected to an initial isothermal stage (5 min at 0°C to stabilize the temperature and state of the samples), followed by heating from 0 to 60°C at 5°C/min. The enthalpy values for endothermic processes were taken as negative and exothermic values as positive.

## **2.4 Particle Size and Zeta Potential**

The particle size and zeta potential of the polymers were determined by dynamic light scattering (DLS) using a Zetasizer Nano ZS (Malvern Instruments Ltd., UK) at a temperature of 37°C. Solutions of both ELRs were prepared by dissolving the ELRs in PBS (pH 7.4) or ultrapure water type I (pH 7.4), when indicated. The solutions were stored at 4°C overnight to allow complete dissolution of the recombinamers and filtered using a 0.45 µm PVDF syringe filter. The samples were then incubated for 30 minutes at 37°C to allow supramolecular assembly to occur and then introduced into polystyrene cuvettes and stabilized for 2 min at the desired temperature. For BSA interaction experiments, ELRs were incubated in 5% BSA PBS for 1, 2 or 3 hours at 37°C after overnight dissolution and then filtered, introduced into polystyrene cuvettes and stabilized for 2 min at the desired temperature. Autocorrelation functions were used to obtain the size distribution and polydispersity index. Z-average mean (nm) and zeta potential (mV) were used for data analysis. Three different samples were analyzed.

## **2.5 Transmission electron microscopy (TEM)**

Solutions were prepared by dissolving the ELRs in ultrapure water type I and kept at 4 °C overnight to allow complete dissolution of the polymers. The sample was incubated for 30 minutes at 37 °C to allow supramolecular assembly to occur, stained with uranyl acetate solution (1,0 wt %) to enhance the contrast of the nanoparticles on a carbon-coated copper

grid, followed by solvent evaporation. Samples were observed using a JEM-2200 electron microscope operating at 200 kV.

## **2.6 Surface Tension by Pendant Drop Technique**

The critical micellar concentration (CMC) of the different ELR solutions in both PBS and ultrapure water type I was determined from surface tension measurements derived from a drop-shape analysis using the pendant drop technique.<sup>33</sup> The changes in the shape of the resulting drop at the air/water interface upon increasing the ELR concentration previously stabilized at 37 °C for 15 min from a blank solution to 20 µM were monitored using the SCA 20 software of a Data Physics OCA20 instrument, which scaled the profile of the drop hanging from a straight precision dosing needle. The drops (4 µL at 0.5 µL/s) were infused using a 500 µL Gastight Hamilton syringe. Three drops were analyzed per condition and the CMC was determined from the point of slope change after plotting the change in surface tension values versus log(concentration) of the ELRs.

## **2.7 Cell culture**

MCF-7 and Caco-2 cells were maintained in MEM supplemented with 10% FBS, 2 mM glutamine, 1% NEAA, 100 U/mL penicillin and 0.1 mg/mL streptomycin at 5% CO<sub>2</sub> and 37 °C. MDA-MB-231 cells were cultured in L-15 medium supplemented with 10% FBS, 100 U/mL penicillin and 0.1 mg/mL streptomycin at 0% CO<sub>2</sub> and 37 °C. hMSC and HFF-1 cells were cultured in DMEM supplemented with 100 U/mL penicillin, 0.1 mg/mL streptomycin and 10% or 15% FBS, respectively, at 10% CO<sub>2</sub> and 37 °C. HUVEC cells were grown in Medium 200 supplemented with 1% gentamicin/amphotericin and LSGS at 5% CO<sub>2</sub> and 37 °C. When required, cells were detached using a solution of 0.05% Trypsin-EDTA. Cells were seeded onto 96-well plates at a quantity of  $2 \times 10^4$  cells per cm<sup>2</sup> for tumor cells and  $1 \times 10^4$  cells

per cm<sup>2</sup> for primary cells, in order to maintain the same levels of confluence for all the cell lines overnight prior to the treatment.

## **2.8 Fluorescence microscopy**

MDA-MB-231 cells were treated with fluorescein-conjugated ELRs at 0.5 mg/mL for 90 minutes. Fluorescence images were taken using a Nikon eclipse Ti-SR (Japan) fluorescence microscope. Cellular nuclei were stained with DAPI.

## **2.9 Cell Viability**

MCF-7, MDA-MB-231, Caco-2, hMSC, HFF-1 and HUVEC were treated with ELRs at three different concentrations (0.25, 0.5 and 1 mg/mL) for different times (30, 60, 90 and 120min). Live and dead staining (LIVE/DEAD Viability/Cytotoxicity Assay Kit, Invitrogen) was used according to the manufacturer's instructions. Briefly, a stock solution of the LIVE/DEAD reagents (1  $\mu$ M calcein AM and 2  $\mu$ M EthD-1 in 10 mL of DPBS) was prepared, samples (100  $\mu$ L) were distributed in each well and incubated for 20 minutes in the dark, then the fluorescence intensity emission was measured at 525 and 645 nm after excitation at 485 and 525 nm (SpectraMax M5e Molecular Devices microplate reader). Additionally, photographic images of cultures were taken using a Nikon eclipse Ti-SR (Japan) fluorescence microscope. Three independent experiments, each in triplicate, were performed.

## **2.10 Western Blot**

Caco-2 and MDA-MB-231 cells were incubated with complete medium containing nanoparticles at 0.5 mg/mL for 2 hours. Cells were lysed and protein concentrations measured using Bradford's reagent. Thus, 50  $\mu$ g of protein was separated using standard SDS-PAGE and transferred to PVDF membranes. Blocking was performed with 5% defatted

dry milk in PBS (pH 7.4) for 1 h at room temperature. Primary Akt, p-Akt and GAPDH antibodies were used in PBS with 0.5% defatted dry milk and 0.1% Tween-20 at 1:1000 and 1:2000, respectively, according to the manufacturer's instructions. After extensive washing, secondary HRP-linked antibodies were used at a 1:10,000 dilution. Specific proteins were visualized using the ECL chemoluminescent substrate.

### **2.11 Apoptosis/Necrosis Assay**

Caco-2 and MDA-MB-231 cells were incubated with complete medium containing nanoparticles at 0.5 mg/mL for 2 hours. FITC-conjugated annexin V and propidium iodide staining (Annexin V FITC Assay Kit, Cayman Chemical) was used according to the manufacturer's instructions, and the fluorescence intensity emission was measured (SpectraMax M5e Molecular Devices microplate reader) at 535 and 595 nm after excitation at 488 and 560 nm, respectively. Three independent experiments, each in triplicate, were performed.

### **2.12 Assessment of Internalization Pathway**

Caco-2 and MDA-MB-231 cells were pre-treated with 25  $\mu$ M chloroquine, 1  $\mu$ g/mL filipin, 5  $\mu$ g/mL amiloride, and 100  $\mu$ M monodansylcadaverine in minimal medium for 30 min. After treatment with inhibitor, the medium was replaced with a fresh one containing 0.5 mg/mL polymer for 2 hours. Finally, the cell viability assay was carried out as described above. Three independent experiments, each in triplicate, were performed.

### **2.13 Assessment of Intracellular Trafficking**

Caco-2 and MDA-MB-231 cells were pre-incubated with 100  $\mu$ M Pepstatin A at 37°C in each cell culture in complete medium for 16 hours. After Pepstatin A treatment, the medium was replaced with a fresh one containing 0.5 mg/mL polymer for 2 hours. The cell viability was then determined as described above. Three independent experiments, each in triplicate, were performed.

#### **2.14 Statistical analysis**

Data are reported as mean  $\pm$  SD (n = 3). Statistical analysis involved a variance analysis in combination with a subsequent analysis using the Bonferroni method. A p value of less than 0.05 was considered to be statistically significant. \*p < 0.05, \*\*p < 0.01, \*\*\*p < 0.001. Data were handled using the SPSS Statistics software version 20 (IBM).

### **3. Results and Discussion**

#### **3.1 ELR design**

ELRs are able to self-assemble into different structures depending on their composition, with amphiphilic ELR-based diblocks forming vesicles or micelles above their transition temperature.<sup>34</sup> The genetic design of ELRs allows us to control their characteristic Tt below the physiological temperature of 37 °C, thus resulting in coacervate formation. One disadvantage of therapeutic molecules, such as drugs or peptides, is their short circulating half-lives, thus meaning that frequent administration of high concentrations is required to obtain therapeutic level.<sup>35</sup> Therapeutic agents have to pass through several biological barriers to reach the tumor tissue and ensure an effective dose. Furthermore, systemic administration results in high toxicity, especially for healthy tissues.<sup>36-37</sup> ELR-based carriers play an interesting role as regards overcoming all these limitations as they are able to extend the

circulating half-life of therapeutic peptides or drugs and also improve their targeting and pharmacokinetics.

We designed two different polymers, both based on an amphiphilic backbone consisting of a hydrophilic block formed by glutamic acid and a hydrophobic block formed by isoleucine. The glutamic acid block is based on the monomer [(VPGVG)<sub>2</sub>-(VPGEG)-(VPGVG)<sub>2</sub>]<sub>10</sub>, whereas the isoleucine block is based on [VGIPG]<sub>60</sub>. This amphiphilic ELR construct has been shown to self-assemble into highly monodisperse and stable nanovesicles with a size of 55 nm<sup>34</sup>. We also included a small sequence containing three lysine residues, to which different molecules can be attached by covalent binding, at the amino terminus. According to the literature, we expected that our polymers would enter the cell via endosomes and continue to lysosomes,<sup>38</sup> therefore we included an LAEL sequence, a small peptide that undergoes a structural change from random coil to  $\alpha$ -helix after acidification of the pH in the endosome/lysosome (pH 5) and triggers destabilization and permeabilization of the vesicle membrane, thereby allowing endosomal escape, in both polymers.<sup>39</sup> The control ELR construct was designed with an amphiphilic backbone containing the three lysine residues and the LAEL sequence. This construct was only used as a polymer control in order to clarify any effect of the ELR modules. Moreover, the LAEL sequence was included in the control polymer in order to study possible cytotoxicity due to internalization of the nanoparticles and their escape from endosomes/lysosomes. Furthermore, we added different bioactive blocks to the functional polymer. For example, cathepsin D (CatD) is a lysosomal aspartyl endopeptidase<sup>40</sup> that is overexpressed in cancer cells compared to normal cells and is thought to promote tumor invasion and growth. As such, we included a cathepsin D-sensitive sequence in order to allow its enzymatic action and Akt inhibitor to reach the cytoplasm. In order to allow the Akt inhibitor to escape from the endosome/lysosome, we added the H5

codifying sequence, a histidine-rich peptide which undergoes a conformational change from a  $\beta$ -structure to a disordered structure at acidic pH<sup>41</sup> as a result of protonation of the imidazole ring in histidine, and provides membrane permeation. Finally, we included the sequence codifying the peptide Akt-in, a small peptide of fifteen amino acids which acts as an inhibitor of protein kinase Akt. Indeed, this inhibitor prevents Ser473-phosphorylation, which is a key step, upon binding to Akt protein<sup>30</sup> before being active in the cellular cytoplasm and playing a key role in multiple signaling pathways.<sup>28</sup> In light of the above, our hypothesis for the mechanism of action is that, once CatD has digested the Cathepsin D-sensitive sequence, the H5 peptide and inhibitor will be released into the cellular cytoplasm and will be able to bind to Akt protein and block it.

The amino acid sequences for the different ELR constructs (control and Akt-in, respectively) are (1) MGKKKPV-LAELLAELLAEL[(VPGVG)2-(VPGEG)10-(VPGVG)2]-[VGIPG]60-V and (2) MGKKKPV-LAELLAELLAEL-[(VPGVG)2(VPGEG)10(VPGVG)2]-[VGIPG]60-VQEYVYD-LFHAI AHFH I HGGWHGLIHGWY-AVTDHPDRLWAWERF-V.

### **3.2 ELR synthesis and bioproduction**

The gene blocks and their intermediate combinations were built by iterative-recursive directional ligation (RDL) from both our own gene library and novel blocks specifically designed and synthesized *ad hoc* for this work, and corroborated by DNA sequencing, as described previously.<sup>31</sup> Plasmids with the final constructs were introduced into the *E. coli* strain BLR(DE3) for expression and synthesis of the polymers. After three heating-cooling purification cycles by sequential inverse transition cycling,<sup>42</sup> the polymers were obtained in a yield of approximately 50 mg/L of bacterial culture. Their molecular weights and purity

were confirmed by SDS-PAGE and MALDI-TOF, respectively. Moreover, the amino acid composition was confirmed by high performance liquid chromatography (HPLC) and nuclear magnetic resonance (NMR). The results are shown in the Supporting Information.

### 3.3 Physical characterization

ELRs are characterized by a thermosensitive behaviour that can be useful for performing controlled drug delivery, thus meaning that the self-assembling ability of ELRs makes them an interesting alternative for the development of biomedical devices. Consequently, the availability of ELR-based delivery systems with a Tt below the physiological temperature is extremely important for our purposes due to the fact that nanoparticles would be formed in the human body.<sup>43</sup>

<b>Polymer</b>	<b>Predicted Molecular Weight (Da)</b>	<b>Experimental Molecular Weight (Da)</b>	<b>Tt (°C)</b>	<b>Endotoxin level (EU/mg)</b>
Control ELR	48250	48180	15.15	0.27
Akt-in ELR	55330	55540	14.58	0.25

**Table 1.** Characterization of ELR polymers. The experimental molecular weights were determined by MALDI-TOF/MS. Transition temperatures (Tt) for polymers dissolved in PBS buffer (pH 7.4) were measured by differential scanning calorimetry (DSC).

The thermal behaviour of both ELRs was measured by DSC in PBS. As can be seen from Table 1, both polymers were found to behave as self-assembling smart systems with a Tt of approximately 15°C, which corresponds to the transition of the hydrophobic block forming the nanoparticle core. These transition temperatures are very similar to those previously exhibited by amphiphilic blocks containing isoleucine and able to self-assemble into nanoparticles.<sup>34</sup> Interestingly, there are few differences between the Tt of both polymers

despite their different composition, thus meaning that the bioactive sequences added to the polymer carrying the Akt inhibitor do not affect their transition temperature. This means that they could be used for biomedical applications because, at body temperature of 37°C, both ELR-based polymers self-assemble. Once the Tt of both polymers had been determined, nanoparticle formation had to be checked because the non-ELR block could prevent self-assembly of the polymers.

Nanoparticle	Size (nm)	PDI	Zeta Potential (mV)	CMC	
				mg/mL	μM
Control NP	65.60 ± 3.73	0.087	-27.8 ± 1.5	0.25	4.49
Akt-in NP	72.46 ± 3.52	0.079	-26.2 ± 1.2	0.21	4.21

**Table 2.** Characterization of ELR nanoparticles. Size and polydispersity index of self-assembled polymers dissolved in PBS measured by dynamic light scattering (DLS). Surface charge of self-assembled polymers dissolved in ultrapure water type I measured by dynamic light scattering (DLS). The CMC was calculated from the surface tension using the pendant drop technique. Mean ± SD.

The nanotechnological approach to cancer therapy takes advantage of the multiple abnormalities inherent to tumor vasculature, such as hypervascularization, aberrant vascular architecture, enhanced production of vascular permeability factors, and the lack of lymphatic drainage.<sup>21-23</sup> Thus, nanocarriers can selectively extravasate into tumor tissues due to their abnormal vascular nature and are subsequently not efficiently removed, thus remaining retained therein.<sup>44</sup> The ideal size for a nanoparticle depends on several factors. First of all, for significant extravasation from fenestrations in the tumor vasculature, nanocarriers need to be smaller than 400 nm.<sup>24</sup> Secondly, particles bigger than 200 nm are likely to be sensitive to macrophages and undergo opsonization.<sup>45</sup> As such, in order to avoid specific capture by the liver, they should be less than 100 nm in size<sup>46</sup> but larger than 10 nm to avoid filtration

by the kidneys.<sup>47</sup> For all these reasons, nanoparticles with a size of 10-100 nm are preferred because of the enhanced permeability and retention effect (EPR).<sup>24</sup> The EPR effect relies on the fact that tumors show abnormal vasculature, which means that nano-size drugs are accumulated in the tumors and show differential accumulation and therefore higher concentrations when compared to the plasma or other organs with proper vasculature. In our work, both polymers exhibited an ability to form nanoparticles, with an average size of 66 nm for the control polymer and 72 nm in the case of the Akt-in ELR, with low PDIs in both cases. This difference in size between the two nanoparticles is statistically relevant and bigger than for previous nanoparticles (55 nm) under the same conditions.<sup>34</sup> The size and morphology were corroborated by TEM, cryo-TEM and fluorescence microscopy images (Figure 1). As these previous nanocarriers consisted only of the amphiphilic ELR backbone, this difference with respect to our new nanoparticles is mainly due to the additional functional peptides. To a lesser extent, the presence of the three bioactive sequences also results in a slight increase in the size of the Akt-in nanoparticles (72 nm). We can therefore conclude that both nanoparticles (control and those carrying the Akt inhibitor) meet all the size requirements for reaching the tumor in a controlled manner, as explained above. Furthermore, both control and Akt-in nanoparticles showed the same size when incubated with BSA (Table S2). This could mean that nanoparticles remain stable in systemic circulation and are not affected by plasmatic protein, such as albumin.

The critical micellar concentration (CMC) was also studied in order to determine the concentration above which ELRs self-assemble into nanoparticles. The pendant drop method showed that both polymers have their CMC in PBS buffer between 0.21 mg/mL (4.21  $\mu$ M) for nanoparticles carrying the Akt inhibitor and 0.25 mg/mL (4.49  $\mu$ M) for control

nanoparticles, as shown in Supplementary figure S7. This difference again highlights the fact that the presence of bioactive sequences does not affect the association and self-assembling ability of ELR-based nanoparticles. Experimental measurements are shown in Supplementary material (figure S4-7).

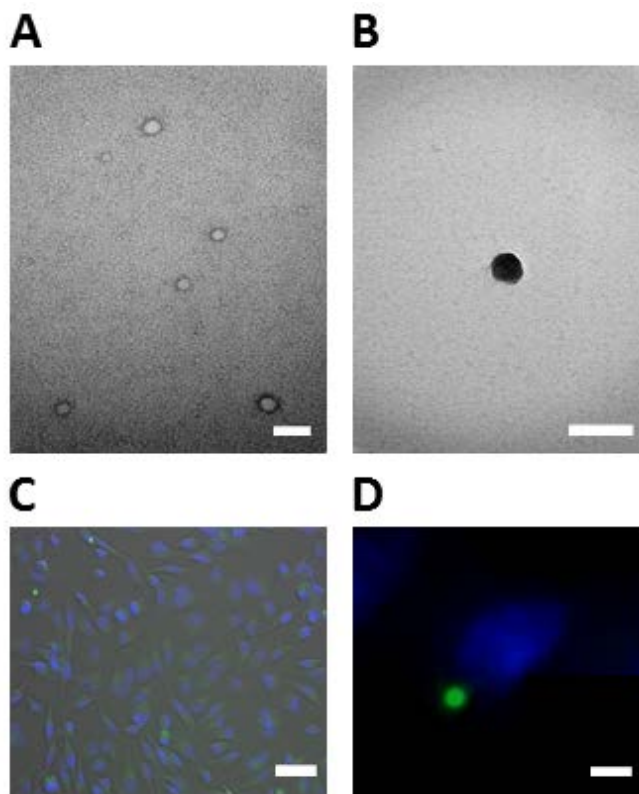


**Figure 1.** Characterization of ELR nanoparticles. TEM images of self-assembled nanoparticles stained with 1% uranyl acetate. A: TEM images of self-assembled nanoparticles stained with 1% uranyl acetate. B: cryo-TEM images of self-assembled nanoparticles stained with 1% uranyl acetate. C: Fluorescence images of self-assembled nanoparticles with conjugated fluorescein. D: Higher magnification of fluorescence images of self-assembled nanoparticles with conjugated fluorescein. Cell nuclei were stained with DAPI. Scale bars: 100 nm for A and B, 50  $\mu\text{m}$  for C and 2  $\mu\text{m}$  for D.

The surface charge of nanoparticles is of marked importance as regards the electrostatic interactions between nanoparticles and the cellular membrane and evaluating nanoparticle

stability. Due to the negative component of the cellular membrane, cationic particles are typically preferred in order to nonspecifically enter into cells by generating holes and inducing local disorders in the membrane,<sup>48</sup> while anionic particles strongly influence membrane structures.<sup>49</sup> However, anionic and neutral nanoparticles are thought to enter cells via endocytic pathways. Moreover, positively charged nanoparticles result in membrane depolarization, which reduces the viability of normal cells, thus having a stronger disruptive ability on the lipid bilayer of the cellular membrane.<sup>50</sup> Furthermore, neutral and negatively charged nanoparticles are able to enter into the lymphatic system better than cationic carriers, which are more likely to form aggregates with interacting proteins, whereas neutral and anionic particles are thought to avoid renal clearance more efficiently.<sup>51</sup> The zeta potential, which determines the surface charge of the nanoparticles, was found to be clearly negative (-27 mV) due to the presence of glutamic acid residues at the nanoparticle surface. Despite the presence of three lysine residues in the corona, the zeta potential was not altered when compared to previous nanoparticles containing the same amphiphilic backbone reported by García-Arévalo *et al.*<sup>34</sup> Thus, these three lysine residues did not affect the nonspecific internalization of nanoparticles by electrostatic interactions with the cellular membrane. Moreover, the bioactive sequences of nanoparticles carrying the Akt inhibitor did not alter the zeta potential compared to control nanoparticles containing the ELR amphiphilic backbone, thus suggesting that bioactive domains are located at the nanoparticle core. Interestingly, both ELR-based nanoparticles showed stable zeta potential when incubated with BSA (Table S2). This could mean that nanoparticles did not interact with albumin, which is the main protein in the plasma, and remain stable in systemic circulation.

### **3.4 Effect of nanoparticles on cell viability**

The main objective of this work was to develop a novel smart drug delivery system in order to achieve an accurate release of an Akt inhibitor, which was designed to trigger apoptosis-mediated death of cancerous cells. Thus, based on different expression levels of Akt protein between cancerous and normal cells, the ELR- based nanoparticles were expected to show enhanced effect on cell viability of cancerous cells, compared to normal ones. Once the nanoparticles had been physically characterized, their biological effect on three human cancer cell lines (Caco-2 epithelial colon carcinoma, and two breast cancer lines: MCF-7 and MDA-MB-231) and three normal human primary cell lines (HFF-1 fibroblasts, hMSCs (mesenchymal stem cells) and HUVEC endothelial cells) was examined. Human cancer cell lines were used for this purpose because of their higher expression of Akt protein than normal human cell lines. Furthermore, cancer cells are known to show higher internalization rates due to their faster metabolic state. We used three different concentrations of nanoparticles ranging from the critical micellar concentration (CMC) of 0.25 mg/mL to 1 mg/mL. As shown in the figures 2 and S8, the viability of cells exposed to three different concentrations of both types of particles was studied at increasing incubation times. First of all, we determined the cytotoxic effect of control nanoparticles (Figure S8). Although this type of nanoparticle did not carry any bioactive sequence, internalization could affect cellular viability by destabilizing the membrane. Incubation with control nanoparticles did not significantly affect the viability of any of the six cell lines studied. Indeed, the results showed no difference between either the three different concentrations studied or between the different time points (from 30 to 120 min). Thus, we can conclude that, under the experimental conditions used, the control system does not cause a decrease in the viability of either cancerous or non-cancerous cells. This lack of effect could happen either because control nanoparticles are not internalized or because they do not affect cell viability. As both

types of nanoparticles have the same surface components, we expected the same internalization rates, thus meaning that we can conclude that control nanoparticles do not compromise cell viability as they are completely innocuous.

Akt-in nanoparticles also showed no effect on the viability of non-cancerous human cells at lower concentrations (Figures 2 and 3). Thus, endothelial cells, mesenchymal cells and fibroblasts were only slightly affected when incubated for 120 minutes with nanoparticles at the highest concentration (1 mg/mL), with cell viability decreasing to 71%, 83% and 77%, respectively. Furthermore, there were no significant differences between non-cancerous cells treated with 0.25 and 0.5 mg/mL nanoparticles carrying the Akt inhibitor at any time. Of the three normal cell lines used, HUVEC cells were the most affected. These results are in accordance with the literature as vascular cells are the most sensitive healthy cells due to their contact with nanoparticles during systemic administration.<sup>52</sup> In light of the above, we have provided evidence that the effect of nanoparticles on cell viability is both time- and concentration-dependent. Indeed, there were no significant differences between the viability of normal cells with a concentration of 0.25 and 0.5 mg/mL at any time point.

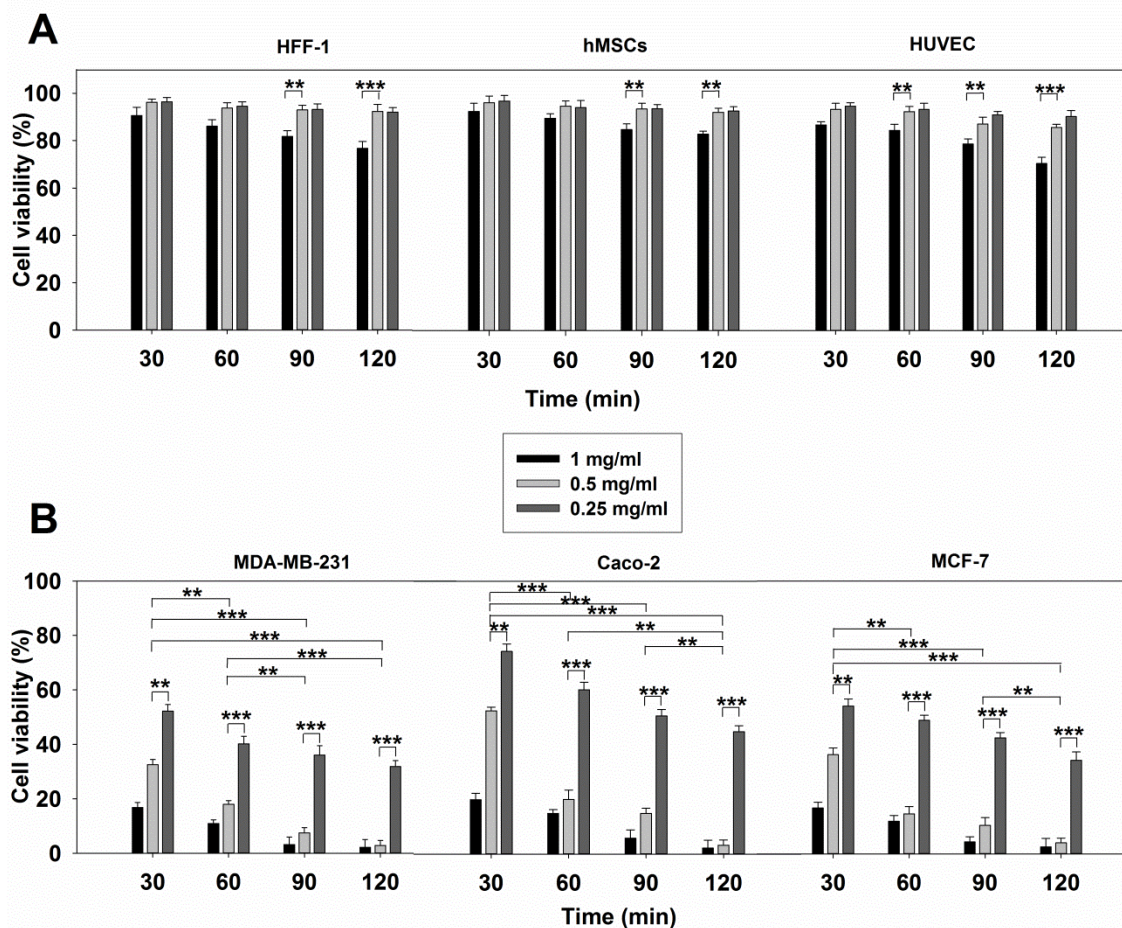


**Figure 2.** Percentage viability for HFF-1, hMSCs and HUVEC (panel A) and MDA-MB-231, Caco-2 and MCF-7 (panel B) with respect to untreated cells. Cells were incubated with Akt-in nanoparticles at three concentrations and times and viability was measured using the LIVE/DEAD assay kit. n = 3 independent experiments, mean ± SD. \*\*p < 0.01; \*\*\*p < 0.001.

In contrast, when cancer cell lines were incubated with nanoparticles carrying the detachable Akt inhibitor, cell viability was strongly affected (Fig. 2). Thus, the viability of cancer cells decreased to less than 20% and 40% after incubation with 0.5 and 1 mg/mL for only 30 minutes, respectively, thus indicating the rapid internalization of these Akt-in NPs. After incubation for 120 minutes, the minimal dose tested, which also corresponds to the CMC of the nanoparticles (Figure 2B), resulted in the death of 55-65% of cancerous cells. Similarly, when the nanoparticle concentration was increased to 0.5 and 1 mg/mL, the effect on cancer

cells was markedly higher (cell viability of 4% and 8% respectively). Thus, an increase in the concentration of Akt-in nanoparticles results in a marked reduction in cell survival. This result suggests that this concentration is the minimal dose able to affect 50% cell viability. These findings also show that, of the three cancer cell lines studied, Caco-2 cells are more resistant to treatment with nanoparticles. These differences could be due to the fact that these cell lines have different internalization rates. Interestingly, the 0.5mg/mL concentration strongly affected the viability of cancer cells without affecting normal cells, therefore this intermediate concentration was used for subsequent experiments because it seemed to be the largest therapeutic window in which significant differences in the viability of normal cells when compared to cancerous cells were observed. This is of particular importance as it could allow control by modulating the concentration. The enhanced action of nanoparticles on cancer cell lines when compared to normal cell lines could also be due to the fact that cancer cells are better able to internalize nanoparticles, as demonstrated by Villanueva et al.<sup>53</sup>

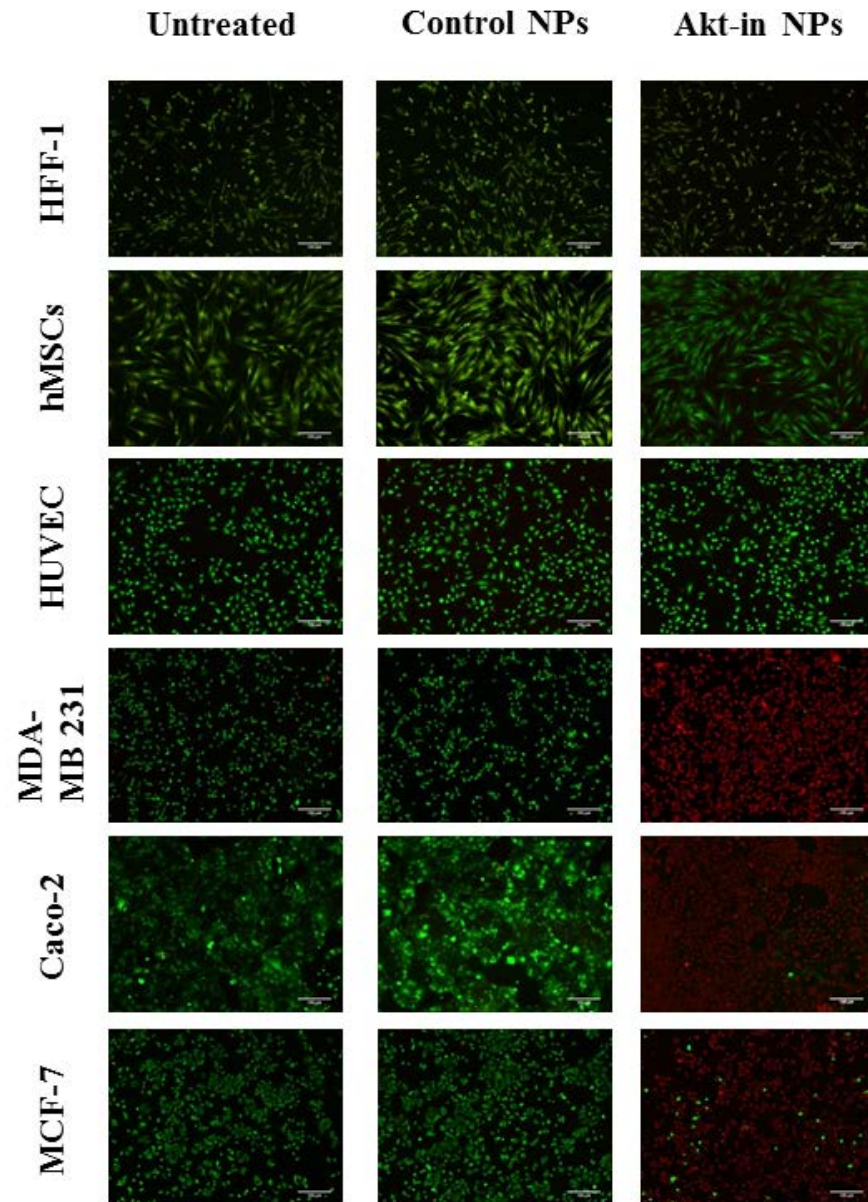


**Figure 3.** Representative fluorescence microscopy images for HFF-1, hMSCs, HUVEC, MDA-MB-231, Caco-2 and MCF-7 cells after incubation with control nanoparticles or Akt-in nanoparticles. Cells were incubated with Akt-in nanoparticles 0.5 mg/mL for 120 minutes and viability was measured using the LIVE/DEAD assay kit. Scale bars are 100  $\mu$ m.

### 3.5 Inhibition of Akt phosphorylation

Akt kinase is activated, in response to multiple stimuli, such as growth factors, by phosphatidyl inositol triphosphate products generated by PI3K. These lipid products bind to

Akt and induce a conformational change in Akt, thus allowing PDK1 to phosphorylate threonine 308. Moreover, phosphorylation of serine 473 and membrane anchoring are required after threonine 308 phosphorylation for final activation of Akt kinase.<sup>28</sup> As we explained above, the mechanism of action of the small peptide inhibitor involved attachment to the Akt kinase, thereby avoiding the phosphorylation of Ser473.<sup>30</sup> In order to confirm the specific effect of the peptide inhibitor, immunoblotting assays were performed in Caco-2 and MDA-MB-231 cells after treatment with Akt-in nanoparticles for 2 hours at 37°C. As can be seen from figure 4, Akt phosphorylation was not altered when cancer cell lines were incubated with control nanoparticles. However, when both cell lines were treated with nanoparticles carrying the inhibitor, phosphorylation of Akt protein at Ser473 was prevented. Consequently, we can conclude that the effect of Akt-in nanoparticles on cell viability is due to the accurate inhibitor delivery and its consequent anti-phosphorylation activity, as expected.

Treatment	Caco-2			MDA-MB-231		
	-	+	-	-	+	-
Control NP	-	+	-	-	+	-
Akt-in NP	-	-	+	-	-	+

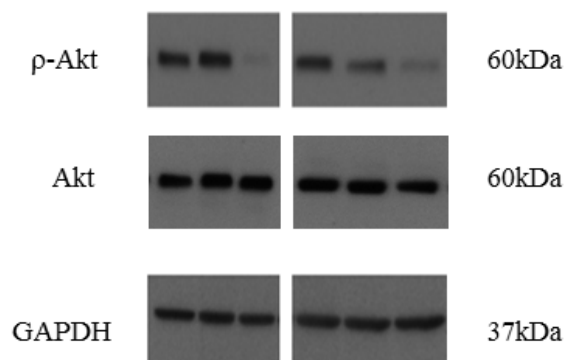


**Figure 4.** Inhibition of Akt phosphorylation triggered by nanoparticles in MDA-MB-231 and Caco-2 cell lines. Cells were incubated with control and Akt-in nanoparticles, and an immunoblot was performed to measure Akt phosphorylation at Ser473, Akt and GAPDH expression, which was used as load control.

### **3.6 Apoptotic death triggered by nanoparticles**

As shown above, ELR nanoparticles were able to provoke cancer cell death under the conditions tested, therefore the next step was to determine the death pathway provoked. There are two major types of cell death: necrosis and apoptosis. Different diseases, including cancer, deregulate this apoptotic process, thereby resulting in pathological conditions.<sup>54</sup> For this reason, analysis of the signaling pathways that control apoptosis is of great importance for drug discovery and for investigating their therapeutic potential. Akt kinase plays a key role in several multiple signaling pathways involving anti-apoptotic effects.<sup>26</sup> Thus, upon blocking Akt kinase, cells should follow the apoptotic pathway and die. Hiromura *et al.*<sup>30</sup> demonstrated that Akt-in compromised Akt-dependent cellular proliferation and the anti-apoptosis role of Akt. For that reason, apoptotic and necrotic cell percentages were determined in Caco-2 and MDA-MB-231 cells after treatment with nanoparticles carrying Akt-in for 2 hours at 37°C. As figure 5 shows, apoptosis was the most commonly triggered death pathway for both cancer cell lines. The experiment with Caco-2 cells showed that 95% of cells were in an apoptotic state and only 5% of dead cells in a necrotic state, whereas the experiment with MDA-MB-231 breast cancer cells confirmed that most cells died by apoptosis (93%) instead of necrosis (7%).

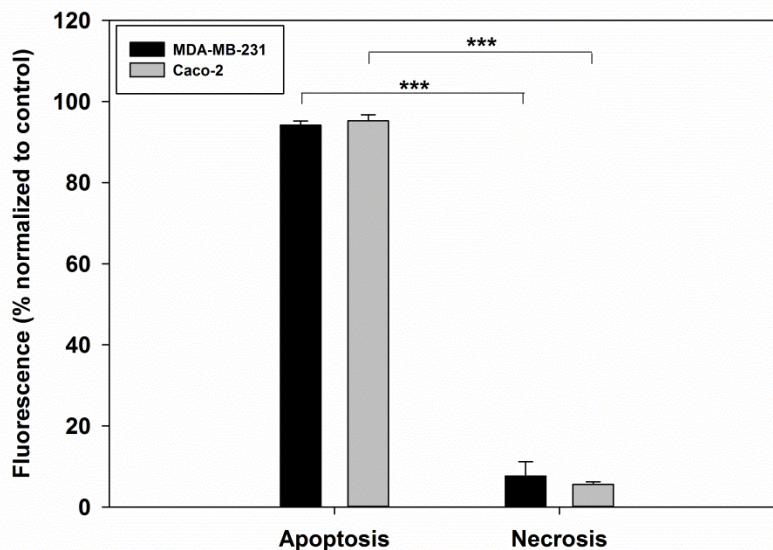


**Figure 5.** Cell-death pathways triggered by nanoparticles in MDA-MB-231 and Caco-2 cell lines. Cells were incubated with the nanoparticles carrying Akt inhibitor, and an apoptosis/necrosis assay was performed for all samples. H<sub>2</sub>O<sub>2</sub> and Triton X-100 treated cells were considered as 100% apoptosis and necrosis control, respectively. n = 3 independent experiments, mean ± SD. \*\*\*p < 0.001.

Thus, both cancer cell lines corroborated that the Akt inhibitor unlocked the apoptotic pathway blocked by Akt kinase. This is of particular importance as it shows that our ELR-based nanoparticles enhance the apoptotic pathway instead of being a pathologic agent for cells.

### 3.7 Endocytic internalization of nanoparticles

Once the specificity of the Akt-in nanoparticles in cancer cell lines had been assessed, their internalization pathway was studied. In general, the internalization pathway for nanoparticles occurs via two mechanisms: phagocytosis and endocytosis.<sup>55</sup> As mentioned above, larger nanoparticles (200 nm) are more likely to undergo phagocytosis whereas smaller ones enter cells by endocytosis. Three different types of endocytosis have been described: macropinocytosis, clathrin-mediated endocytosis (CME) and caveolae-mediated endocytosis

(CvME),<sup>38</sup> but only the latter two mechanisms work via receptor-ligand interactions forming vesicles that are invaginated, such as endosomes and lysosomes.<sup>38, 56-57</sup> In our case, internalization of the NPs via an endocytic mechanism is critical in order to allow the Akt inhibitor to reach the cytoplasm after the participation of lysosomal enzyme Cathepsin D and H5 peptide for endolysosomal escape. Of the six cell lines used above, Caco-2 and MDA-MB-231 were selected to determine the internalization pathway due to their higher levels of Akt expression and the different activity of the Akt-in nanoparticles observed. This selection could give us a better insight into the accuracy and mechanism of action of the nanoparticles when faced with cancer cells in which Akt kinase is overexpressed. As such, this selection could be the most realistic *in vitro* scenario for our study prior to using *in vivo* models in future studies. To determine this, Caco-2 and MDA-MB-231 cells were pre-treated with four different endocytosis inhibitors for 30 min at 37°C and then incubated with Akt-in nanoparticles for 2 hours at 37°C. Maximum viability (positive control) was achieved when cells were treated with PBS for 2 hours, whereas the negative control was achieved with Akt-in NPs instead of PBS. As can be seen from figures 6 and 7, the inhibition of macropinocytosis by amiloride (Na<sup>+</sup>/H<sup>+</sup> exchange) did not alter the effect of nanoparticles on cell viability, whereas the inhibition of caveolae-mediated endocytosis by filipin only showed a minimum but statistically significant effect (14% cell viability). However, the inhibition of clathrin-mediated endocytosis by monodansylcadaverine was found to almost completely inhibit the action of nanoparticles and a cell viability of 92% was restored. Additionally, the inhibition of acidification in acidic vesicles by chloroquine also significantly affected (80% cell viability) the action of nanoparticles.

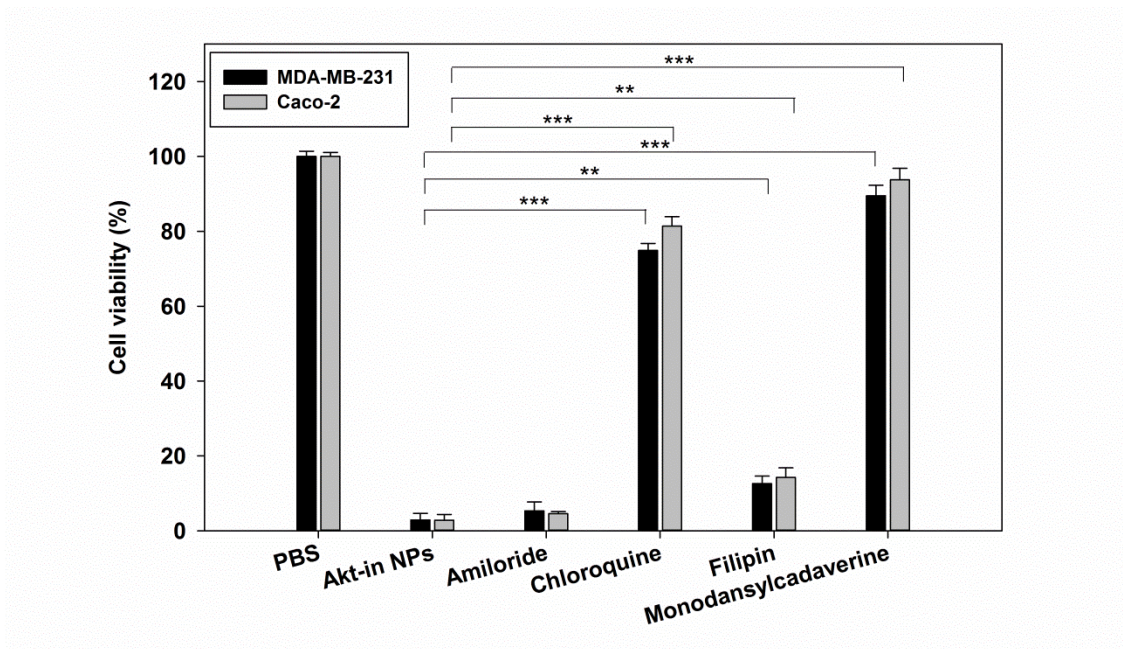


**Figure 6.** Study of the internalization pathways for nanoparticles carrying Akt inhibitor in MDA-MB-231 and Caco-2 cell lines. Cells were incubated with PBS (100% viability), 0.5 mg/mL Akt-in nanoparticles (0% viability) or pre-incubated with an internalization inhibitor, such as amiloride, chloroquine, filipin or monodansylcadaverine prior to treatment with 0.5 mg/mL Akt-in nanoparticles. Viability was measured using the LIVE/DEAD assay kit.  $n = 3$  independent experiments, mean  $\pm$  SD. \*\* $p < 0.01$ ; \*\*\* $p < 0.001$ .

These findings show the primary influence of clathrin-mediated endocytosis for the internalization of nanoparticles, due to the action of the enzyme Cathepsin D on the CatD-sensitive sequence in order to release the Akt inhibitor. We have also demonstrated the importance of endosomal/lysosomal acidification for our nanoparticles as this acidification allows the conformational change and action of H5 peptide in order to escape from acidic vesicles. All these results may also suggest that lysosomes are key actors in the intracellular activation of nanoparticles as, if the nanoparticles underwent a different internalization pathway, they would not be effective.

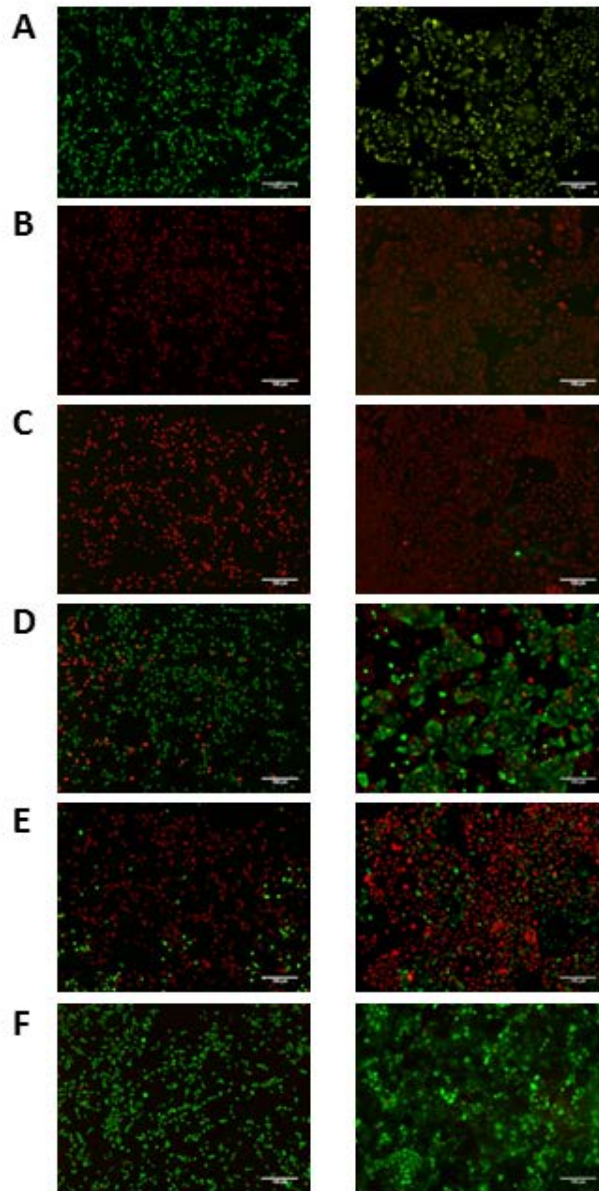


**Figure 7.** Representative fluorescence microscopy images for Caco-2 (right) and MDA-MB-231 (left) after incubation with A: PBS (100% viability) B: 0.5 mg/mL Akt-in nanoparticles (0% viability) or pre-incubated with an internalization inhibitor, such as: C: amiloride D: chloroquine E: filipin or F: monodansylcadaverine prior to treatment with Akt-in nanoparticles. Cells were incubated with endocytosis inhibitors for 30 min before the treatment with Akt-in nanoparticles 0.5 mg/mL for 120 minutes and viability was measured using the LIVE/DEAD assay kit. Scale bars are 100  $\mu$ m.

### **3.8 Intracellular nanoparticle activation**

One of the most promising advantages of genetically engineered ELR-based nanoparticles is the fact that the action on targeted cells and tissues can be modulated by adding different bioactive functionalities. As shown above, endocytic acidification seemed to be a key factor in nanoparticle activation. Endosome acidification upon fusion with the lysosome also means that multiple degradative enzymes act on the cargo.<sup>58</sup> One of the key lysosomal proteases is the aspartyl endopeptidase Cathepsin D,<sup>59</sup> which shows a higher expression in tumors than in normal tissues and is thought to promote tumor invasion and growth.<sup>40</sup> As such, we included a CatD-sensitive sequence upstream of Akt-in in our polymer in order to allow the inhibitor to be removed from the NP and be released into the cytoplasm after the action of H5 for lysosomal escape, thereby binding to the targeted protein. Thus, as the participation of CatD-directed degradation should be critical for Akt-in activation, we assessed the role of CatD in our system by selectively inhibiting it using Pepstatin A.<sup>60</sup> As such, we hypothesized that when the lysosomal degradative enzyme Cathepsin D is inhibited, the Akt inhibitor peptide cannot be released into the cytoplasm and reach Akt protein in order to block it. The two human cancer cell lines Caco-2 and MDA-MB-231 cells were pre-incubated with 100  $\mu$ M Pepstatin A for 16 hours at 37°C before treatment with Akt-in nanoparticles for 2 hours at 37°C. The cell viability was then assessed. As can be seen from figure 8, incubation of cells with the CatD inhibitor did not produce any effect on cell viability despite blocking an important degradative enzyme. Similarly, when cells were pre-treated with Pepstatin A the nanoparticles also had no effect and cell viability was not affected, in contrast to the effect of nanoparticles in both these cancer cell lines when the action of CatD is not inhibited. We can therefore conclude that Akt-in nanoparticles lose their effect on cell viability when their intracellular activation is inhibited. This could be due to the fact that the peptide is unable to

escape from the lysosome, thus meaning that Akt protein is not reached and continues to enhance cell proliferation and block apoptotic cell death.

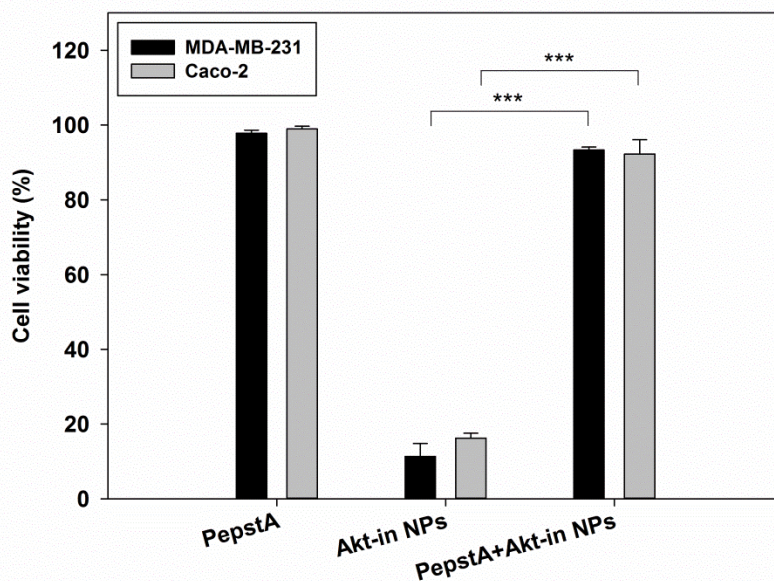


**Figure 8.** Lysosomal trafficking of nanoparticles carrying Akt inhibitor in MDA-MB-231 and Caco-2 cell lines. Cells were incubated with Pepstatin A (negative control), Akt-in nanoparticles or both, and viability was measured using the LIVE/DEAD assay kit.  $n = 3$  independent experiments, mean  $\pm$  SD. \*\*\* $p < 0.001$ .

## **4. Conclusion**

One of the disadvantages of current chemotherapeutic treatments against cancer is the lack of specificity of the drugs, which therefore results in significant damage to healthy tissues.<sup>18</sup> In order to improve the selectivity of new drugs, nanotechnological approaches with incorporated targeting systems appear to be the best strategy.<sup>2</sup> Furthermore, different types of solid tumor offer multiples obstacles to the drug-delivery systems tested to date. Akt kinase is one of the most interesting of the multiple proteins that can be targeted due to its higher expression in cancerous cells and its role as a key factor controlling multiple signalling pathways and processes, such as cell growth, proliferation and survival.<sup>26</sup> The small peptide

inhibitor Akt-in was therefore designed in order to block Akt protein, thereby inhibiting both its essential activity and tumor cell growth.<sup>30</sup>

Thus, we have developed a new smart nanodevice specifically designed including different bioactive peptides so as to achieve the proper delivery of therapeutic agents in targeted cells and tissues. Genetic engineering techniques used for the design of these ELR polymers allows us to be able to create different advanced drug delivery systems with diverse applications as therapeutic approach for multiple diseases, taking advantage of its smart stimuli-responsive behavior. In this work, we have developed a new ELR-based nanoparticle carrying a small peptide inhibitor against Akt protein in order to create an advanced approach for application thereof in the therapeutic treatment of cancer. It should be noted that a complex design of the smart nanoparticles, with different actors, was needed in order to successfully release the inhibitor into the cell cytoplasm, thereby avoiding degradative proteases which would not allow the peptide to enter otherwise.

We tested the specificity of this novel ELR nanoparticle in 6 different cell lines. Thus, our drug delivery system showed no effect in three primary non-cancerous cell lines, while the same treatment showed lethal effects in breast and colorectal cancerous cells. Moreover, *in vitro* experiments confirmed that each block included in the polymer was absolutely required for the proper release of the inhibitor in the cellular cytoplasm. Thus, inactivation of lysosomal proteases and inhibition of vesicles acidification resulted in abolished effect of nanoparticles.

Overall, based on our findings, we can conclude that this smart nanodevice could be a novel strategy for the proper release of therapeutic agents at molecular level in targeted cells. This study is the first to report an accurate smart nanodevice against Akt protein after intracellular

activation. Interestingly, our system improved the accuracy of the inhibitor in a time- (our system was 12 times faster than the inhibitor alone) and dose-dependent manner (5 times lower amount of inhibitor), compared to previous works with Akt-in.<sup>30</sup> This improved action of Akt-in when carried in nanoparticles could be due to the better internalization of nanoparticles compared to nude peptides and their shielding effect, which protects the inhibitor from cellular proteases.

It is worthy to mention that our new therapeutic system is not limited to one type of cancer, as it is targeted to Akt kinase protein, which is overexpressed in multiple neoplastic diseases, such as colon, pancreatic, breast, ovarian and lung cancer. Further studies are needed to study the accuracy of these nanoparticles in *in vivo* models better resembling the tumor environment and its interactions with nanocarriers. In the future, patients overexpressing Akt may be candidates for therapeutic treatment with nanoparticles bearing the inhibitor, which could improve the problems caused by current non-specific chemotherapeutic drugs.

### **Supporting Information**

Amino acid sequence of polymers (Table S1), SDS-PAGE of ELRs purification (Figure S1), High Performance Liquid Chromatography (HPLC) and Mass Spectrometry (MALDI-TOF/MS) analysis of control polymer (Figure S2) and Akt-in polymer (Figure S3), Differential Scanning Calorimetry (DSC) analysis of ELRs (Figure S4), Dynamic Light Scattering analysis of nanoparticle size (Figure S5), Dynamic Light Scattering analysis of nanoparticle zeta potential (Figure S6), Dynamic Light Scattering analysis of nanoparticle size and zeta potential after incubation with 5% BSA (Table S2), Critical Micellar Concentration (CMC) analysis of ELRs using the pendant drop method (Figure S7) and Live/Dead analysis of HFF-1, hMSCs, HUVEC, MDA-MB-231, Caco-2 and MCF-7

incubated with control nanoparticles at three concentrations and times (Figure S8). This material is available free of charge via the Internet at <http://pubs.acs.org>.

### **Corresponding author**

\*Corresponding author: [arias@bioforge.uva.es](mailto:arias@bioforge.uva.es)

BIOFORGE (Group for Advanced Materials and Nanobiotechnology), CIBER-BBN, University of Valladolid, 47011 Valladolid, Spain.

### **Conflict of interest**

The authors declare no competing financial interest.

### **Acknowledgments**

The authors are grateful for financial support from the European Social Fund (ESF) and the European Regional Development Fund (ERDF), as well as funding from the EU (NMP-2014-646075), the MINECO (PCIN-2015-010, MAT2015-68901-R, MAT2016-79435-R and MAT2016-78903-R), the JCyL (project VA317P18), the CIBER-BBN, the JCyL and the Instituto de Salud Carlos III under the "Network Center of Regenerative Medicine and Cellular Therapy of Castilla and Leon". The authors would like to thank R. García for her technical assistance.

## **References**

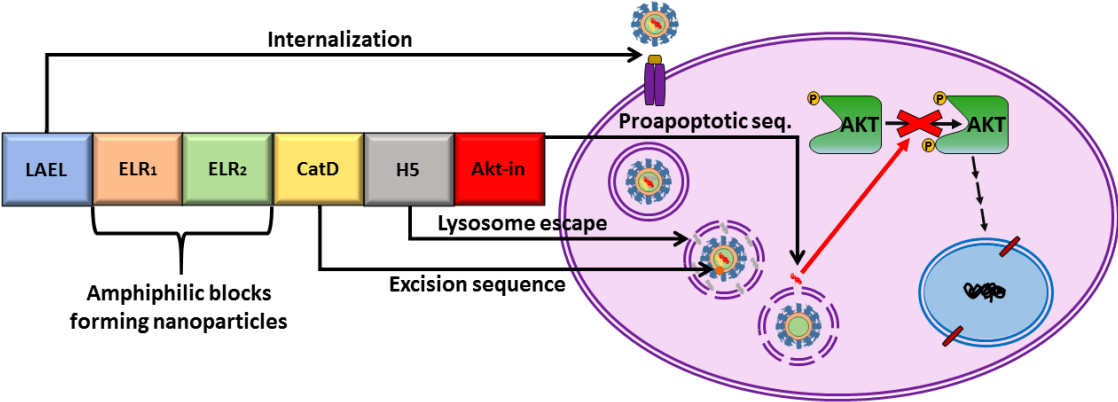
- (1) Saxena, R.; Nanjan, M. J. Elastin-like polypeptides and their applications in anticancer drug delivery systems: a review. *Drug Deliv.* **2015**, *22* (2), 156-67.
- (2) Jain, V.; Jain, S.; Mahajan, S. C. Nanomedicines based drug delivery systems for anti-cancer targeting and treatment. *Curr. Drug Deliv.* **2015**, *12* (2), 177-91.
- (3) Zhang, Y.; Chan, H. F.; Leong, K. W. Advanced materials and processing for drug delivery: the past and the future. *Adv. Drug Deliv. Rev.* **2013**, *65* (1), 104-20.
- (4) Han, W.; Chilkoti, A.; Lopez, G. P. Self-assembled hybrid elastin-like polypeptide/silica nanoparticles enable triggered drug release. *Nanoscale.* **2017**, *9* (18), 6178-6186.
- (5) Shi, J.; Kantoff, P. W.; Wooster, R.; Farokhzad, O. C. Cancer nanomedicine: progress, challenges and opportunities. *Nat. Rev. Cancer.* **2017**, *17* (1), 20-37.

- (6) Raucher, D.; Massodi, I.; Bidwell, G. L. Thermally targeted delivery of chemotherapeutics and anti-cancer peptides by elastin-like polypeptide. *Expert. Opin. Drug Deliv.* **2008**, *5* (3), 353-69.
- (7) Floss, D. M.; Schallau, K.; Rose-John, S.; Conrad, U.; Scheller, J. Elastin-like polypeptides revolutionize recombinant protein expression and their biomedical application. *Trends. Biotechnol.* **2010**, *28* (1), 37-45.
- (8) Shi, P.; Gustafson, J. A.; MacKay, J. A. Genetically engineered nanocarriers for drug delivery. *Int. J. Nanomedicine.* **2014**, *9*, 1617-26.
- (9) Ryu, J. S.; Raucher, D. Elastin-like polypeptide for improved drug delivery for anticancer therapy: preclinical studies and future applications. *Expert. Opin. Drug Deliv.* **2015**, *12* (4), 653-67.
- (10) Rodriguez-Cabello, J. C.; Pina, M. J.; Ibanez-Fonseca, A.; Fernandez-Colino, A.; Arias, F. J. Nanotechnological Approaches to Therapeutic Delivery Using Elastin-Like Recombinamers. *Bioconjug. Chem.* **2015**, *26* (7), 1252-65.
- (11) Rodriguez-Cabello, J. C.; Arias, F. J.; Rodrigo, M. A.; Girotti, A. Elastin-like polypeptides in drug delivery. *Adv. Drug Deliv. Rev.* **2016**, *97*, 85-100.
- (12) Arias, F. J.; Santos, M.; Ibanez-Fonseca, A.; Pina, M. J.; Serrano, S. Elastin-Like Recombinamers As Smart Drug Delivery Systems. *Curr. Drug Targets.* **2018**, *19* (4), 360-379.
- (13) Fernandez-Colino, A.; Quinteros, D. A.; Allemandi, D. A.; Girotti, A.; Palma, S. D.; Arias, F. J. Self-Assembling Elastin-Like Hydrogels for Timolol Delivery: Development of an Ophthalmic Formulation Against Glaucoma. *Mol. Pharm.* **2017**, *14* (12), 4498-4508.
- (14) Mastria, E. M.; Chen, M.; McDaniel, J. R.; Li, X.; Hyun, J.; Dewhirst, M. W.; Chilkoti, A. Doxorubicin-conjugated polypeptide nanoparticles inhibit metastasis in two murine models of carcinoma. *J. Control. Release.* **2015**, *208*, 52-8.
- (15) MacKay, J. A.; Chen, M.; McDaniel, J. R.; Liu, W.; Simnick, A. J.; Chilkoti, A. Self-assembling chimeric polypeptide-doxorubicin conjugate nanoparticles that abolish tumours after a single injection. *Nat. Mater.* **2009**, *8* (12), 993-9.
- (16) McDaniel, J. R.; Callahan, D. J.; Chilkoti, A. Drug delivery to solid tumors by elastin-like polypeptides. *Adv. Drug Deliv. Rev.* **2010**, *62* (15), 1456-67.
- (17) Pina, M. J.; Alex, S. M.; Arias, F. J.; Santos, M.; Rodriguez-Cabello, J. C.; Ramesan, R. M.; Sharma, C. P. Elastin-like recombinamers with acquired functionalities for gene-delivery applications. *J. Biomed. Mater. Res. A.* **2015**, *103* (10), 3166-78.
- (18) Byrne, J. D.; Betancourt, T.; Brannon-Peppas, L. Active targeting schemes for nanoparticle systems in cancer therapeutics. *Adv. Drug Deliv. Rev.* **2008**, *60* (15), 1615-26.
- (19) Hillaireau, H.; Couvreur, P. Nanocarriers' entry into the cell: relevance to drug delivery. *Cell Mol. Life Sci.* **2009**, *66* (17), 2873-96.
- (20) Bae, H.; Chu, H.; Edalat, F.; Cha, J. M.; Sant, S.; Kashyap, A.; Ahari, A. F.; Kwon, C. H.; Nichol, J. W.; Manoucheri, S.; Zamanian, B.; Wang, Y.; Khademhosseini, A. Development of functional biomaterials with micro- and nanoscale technologies for tissue engineering and drug delivery applications. *J. Tissue Eng. Regen. Med.* **2014**, *8* (1), 1-14.
- (21) Torchilin, V. P. Drug targeting. *Eur. J. Pharm. Sci.* **2000**, *11 Suppl 2*, S81-91.
- (22) Matsumura, Y.; Maeda, H. A new concept for macromolecular therapeutics in cancer chemotherapy: mechanism of tumorotropic accumulation of proteins and the antitumor agent smancs. *Cancer Res.* **1986**, *46* (12 Pt 1), 6387-92.
- (23) Maeda, H.; Bharate, G. Y.; Daruwalla, J. Polymeric drugs for efficient tumor-targeted drug delivery based on EPR-effect. *Eur. J. Pharm. Biopharm.* **2009**, *71* (3), 409-19.
- (24) Jain, R. K. Transport of molecules in the tumor interstitium: a review. *Cancer Res.* **1987**, *47* (12), 3039-51.

- (25) Pina, M. J.; Girotti, A.; Santos, M.; Rodriguez-Cabello, J. C.; Arias, F. J. Biocompatible ELR-Based Polyplexes Coated with MUC1 Specific Aptamers and Targeted for Breast Cancer Gene Therapy. *Mol. Pharm.* **2016**, *13* (3), 795-808.
- (26) Cantley, L. C. The phosphoinositide 3-kinase pathway. *Science*. **2002**, *296* (5573), 1655-7.
- (27) Bellacosa, A.; Testa, J. R.; Staal, S. P.; Tsichlis, P. N. A retroviral oncogene, akt, encoding a serine-threonine kinase containing an SH2-like region. *Science*. **1991**, *254* (5029), 274-7.
- (28) Vanhaesebroeck, B.; Alessi, D. R. The PI3K-PDK1 connection: more than just a road to PKB. *Biochem. J.* **2000**, *346 Pt 3*, 561-76.
- (29) Luo, J.; Manning, B. D.; Cantley, L. C. Targeting the PI3K-Akt pathway in human cancer: rationale and promise. *Cancer Cell*. **2003**, *4* (4), 257-62.
- (30) Hiromura, M.; Okada, F.; Obata, T.; Auguin, D.; Shibata, T.; Roumestand, C.; Noguchi, M. Inhibition of Akt kinase activity by a peptide spanning the betaA strand of the proto-oncogene TCL1. *J. Biol. Chem.* **2004**, *279* (51), 53407-18.
- (31) Rodriguez-Cabello, J. C.; Girotti, A.; Ribeiro, A.; Arias, F. J. Synthesis of genetically engineered protein polymers (recombinamers) as an example of advanced self-assembled smart materials. *Methods Mol. Biol.* **2012**, *811*, 17-38.
- (32) Sallach, R. E.; Cui, W.; Balderrama, F.; Martinez, A. W.; Wen, J.; Haller, C. A.; Taylor, J. V.; Wright, E. R.; Long, R. C., Jr.; Chaikof, E. L. Long-term biostability of self-assembling protein polymers in the absence of covalent crosslinking. *Biomaterials*. **2010**, *31* (4), 779-91.
- (33) Fenton, O. S.; Olafson, K. N.; Pillai, P. S.; Mitchell, M. J.; Langer, R. Advances in Biomaterials for Drug Delivery. *Adv. Mater.* **2018**, DOI: 10.1002/adma.201705328
- (34) Garcia-Arevalo, C.; Bermejo-Martin, J. F.; Rico, L.; Iglesias, V.; Martin, L.; Rodriguez-Cabello, J. C.; Arias, F. J. Immunomodulatory nanoparticles from elastin-like recombinamers: single-molecules for tuberculosis vaccine development. *Mol. Pharm.* **2013**, *10* (2), 586-97.
- (35) Kowalczyk, T.; Hnatuszko-Konka, K.; Gerszberg, A.; Kononowicz, A. K. Elastin-like polypeptides as a promising family of genetically-engineered protein based polymers. *World J. Microbiol. Biotechnol.* **2014**, *30* (8), 2141-52.
- (36) MacEwan, S. R.; Chilkoti, A. Applications of elastin-like polypeptides in drug delivery. *J. Control. Release*. **2014**, *190*, 314-30.
- (37) Santos, M.; Serrano-Ducar, S.; Gonzalez-Valdivieso, J.; Vallejo, R.; Girotti, A.; Cuadrado, P.; Arias, F. J. Genetically Engineered Elastin-based Biomaterials for Biomedical Applications. *Curr. Med. Chem.* **2018**.
- (38) Sahay, G.; Alakhova, D. Y.; Kabanov, A. V. Endocytosis of nanomedicines. *J. Control. Release*. **2010**, *145* (3), 182-95.
- (39) Ohmori, N.; Niidome, T.; Wada, A.; Hirayama, T.; Hatakeyama, T.; Aoyagi, H. The enhancing effect of anionic alpha-helical peptide on cationic peptide-mediated transfection systems. *Biochem. Biophys. Res. Commun.* **1997**, *235* (3), 726-9.
- (40) Kirana, C.; Shi, H.; Laing, E.; Hood, K.; Miller, R.; Bethwaite, P.; Keating, J.; Jordan, T. W.; Hayes, M.; Stubbs, R. Cathepsin D Expression in Colorectal Cancer: From Proteomic Discovery through Validation Using Western Blotting, Immunohistochemistry, and Tissue Microarrays. *Int. J. Proteomics*. **2012**, *2012*, 245819.
- (41) Bure, C.; Maget, R.; Delmas, A. F.; Pichon, C.; Midoux, P. Histidine-rich peptide: evidence for a single zinc-binding site on H5WYG peptide that promotes membrane fusion at neutral pH. *J. Mass. Spectrom.* **2009**, *44* (1), 81-9.
- (42) Meyer, D. E.; Chilkoti, A. Purification of recombinant proteins by fusion with thermally-responsive polypeptides. *Nat. Biotechnol.* **1999**, *17* (11), 1112-5.

- (43) Moktan, S.; Perkins, E.; Kratz, F.; Raucher, D. Thermal targeting of an acid-sensitive doxorubicin conjugate of elastin-like polypeptide enhances the therapeutic efficacy compared with the parent compound in vivo. *Mol. Cancer Ther.* **2012**, *11* (7), 1547-56.
- (44) Bouzin, C.; Feron, O. Targeting tumor stroma and exploiting mature tumor vasculature to improve anti-cancer drug delivery. *Drug Resist. Updat.* **2007**, *10* (3), 109-20.
- (45) Owens, D. E., 3rd; Peppas, N. A. Opsonization, biodistribution, and pharmacokinetics of polymeric nanoparticles. *Int. J. Pharm.* **2006**, *307* (1), 93-102.
- (46) Khullar, O. V.; Griset, A. P.; Gibbs-Strauss, S. L.; Chirieac, L. R.; Zubris, K. A.; Frangioni, J. V.; Grinstaff, M. W.; Colson, Y. L. Nanoparticle migration and delivery of Paclitaxel to regional lymph nodes in a large animal model. *J. Am. Coll. Surg.* **2012**, *214* (3), 328-37.
- (47) Davis, M. E.; Chen, Z. G.; Shin, D. M. Nanoparticle therapeutics: an emerging treatment modality for cancer. *Nat. Rev. Drug Discov.* **2008**, *7* (9), 771-82.
- (48) Lin, J.; Zhang, H.; Chen, Z.; Zheng, Y. Penetration of lipid membranes by gold nanoparticles: insights into cellular uptake, cytotoxicity, and their relationship. *ACS Nano.* **2010**, *4* (9), 5421-9.
- (49) Li, Y.; Gu, N. Thermodynamics of charged nanoparticle adsorption on charge-neutral membranes: a simulation study. *J. Phys. Chem. B.* **2010**, *114* (8), 2749-54.
- (50) Arvizo, R. R.; Miranda, O. R.; Thompson, M. A.; Pabelick, C. M.; Bhattacharya, R.; Robertson, J. D.; Rotello, V. M.; Prakash, Y. S.; Mukherjee, P. Effect of nanoparticle surface charge at the plasma membrane and beyond. *Nano Lett.* **2010**, *10* (7), 2543-8.
- (51) Malam, Y.; Loizidou, M.; Seifalian, A. M. Liposomes and nanoparticles: nanosized vehicles for drug delivery in cancer. *Trends. Pharmacol. Sci.* **2009**, *30* (11), 592-9.
- (52) Spencer, D. S.; Puranik, A. S.; Peppas, N. A. Intelligent Nanoparticles for Advanced Drug Delivery in Cancer Treatment. *Curr. Opin. Chem. Eng.* **2015**, *7*, 84-92.
- (53) Villanueva, A.; Canete, M.; Roca, A. G.; Calero, M.; Veintemillas-Verdaguer, S.; Serna, C. J.; Morales Mdel, P.; Miranda, R. The influence of surface functionalization on the enhanced internalization of magnetic nanoparticles in cancer cells. *Nanotechnology.* **2009**, *20* (11), 115103.
- (54) van Engeland, M.; Nieland, L. J.; Ramaekers, F. C.; Schutte, B.; Reutelingsperger, C. P. Annexin V-affinity assay: a review on an apoptosis detection system based on phosphatidylserine exposure. *Cytometry.* **1998**, *31* (1), 1-9.
- (55) Coco, R.; Plapied, L.; Pourcelle, V.; Jerome, C.; Brayden, D. J.; Schneider, Y. J.; Preat, V. Drug delivery to inflamed colon by nanoparticles: comparison of different strategies. *Int. J. Pharm.* **2013**, *440* (1), 3-12.
- (56) Conner, S. D.; Schmid, S. L. Regulated portals of entry into the cell. *Nature.* **2003**, *422* (6927), 37-44.
- (57) Gamboa, J. M.; Leong, K. W. In vitro and in vivo models for the study of oral delivery of nanoparticles. *Adv. Drug Deliv. Rev.* **2013**, *65* (6), 800-10.
- (58) Jovic, M.; Sharma, M.; Rahajeng, J.; Caplan, S. The early endosome: a busy sorting station for proteins at the crossroads. *Histol. Histopathol.* **2010**, *25* (1), 99-112.
- (59) Pranjoli, M. Z.; Gutowski, N.; Hannemann, M.; Whatmore, J. The Potential Role of the Proteases Cathepsin D and Cathepsin L in the Progression and Metastasis of Epithelial Ovarian Cancer. *Biomolecules.* **2015**, *5* (4), 3260-79.
- (60) Amritraj, A.; Wang, Y.; Revett, T. J.; Vergote, D.; Westaway, D.; Kar, S. Role of cathepsin D in U18666A-induced neuronal cell death: potential implication in Niemann-Pick type C disease pathogenesis. *J. Biol. Chem.* **2013**, *288* (5), 3136-52.

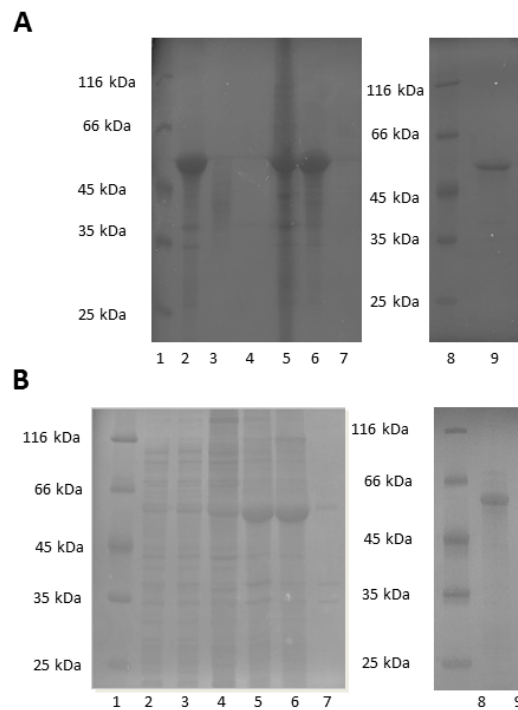
**TOC Abstract:**



## Supplementary material

	<b>3K</b>	<b>LAEL</b>	<b>E<sub>50</sub></b>	<b>I<sub>60</sub></b>	<b>CatD</b>	<b>H5</b>	<b>Akt-in</b>
<b>Control</b>	MGKKKP V	(LAEL) <sub>3</sub>	[(VPGVG) <sub>2</sub> (VPGEG) <sub>10</sub> (VPGVG) <sub>2</sub> ]	[VGIPG] <sub>60</sub>			
<b>Akt-in</b>	MGKKKP V	(LAEL) <sub>3</sub>	[(VPGVG) <sub>2</sub> (VPGEG) <sub>10</sub> (VPGVG) <sub>2</sub> ]	[VGIPG] <sub>60</sub>	VQEYVYD	LFHAI AHF HIHGGWH GLIHGWY	AVTDHP DRLWAW ERF

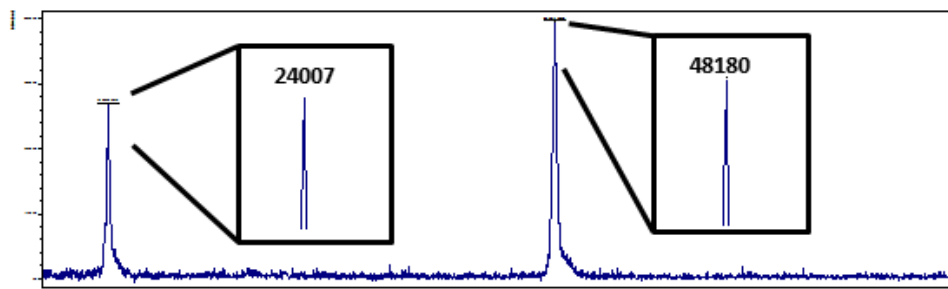
**Table S1.** Composition of polymers. Amino acid sequence of ELR polymers.



**Figure S1.** Characterization of ELR polymers. The expression vectors containing the selected ELR genes were transformed into *Escherichia coli* BLR (DE3) strain for production. The ELR was then bioproduced in *Escherichia coli* in a 15-L bioreactor and purified by several cooling and heating purification cycles (Inverse Transition Cycling) following centrifugation, thereby taking advantage of the ability of these recombinamers to aggregate above their transition temperature. Finally, the polymer was dialyzed against ultrapure water type I and sterilized by filtration (0.22  $\mu$ m filters). A: Purification of control polymer measured by SDS-PAGE. 1: protein marker; 2: cold supernatant; 3: cold pellet; 4: hot supernatant; 5: hot pellet; 6: cold supernatant; 7: cold pellet; 8: protein marker; 9: pure lyophilized polymer. Purification of Akt-in polymer measured by SDS-PAGE. 1: protein marker; 2: production sample; 3: production sample; 4: cold pellet; 5: cold supernatant; 6: hot pellet; 7: hot supernatant; 8: protein marker; 9: pure lyophilized polymer

**A**

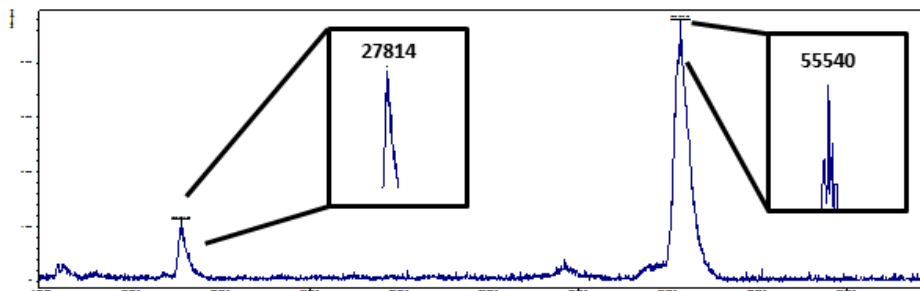
	AA	Mr patron	Experimental		Theoretical
			% masa	count	count
D	ASP+ASN	133.11	0.00	0.00	
E	GLU +GLN	147.13	3.60	14.13	13
N		132.12	0.00	0.00	
S	SER	105.09	0.00	0.00	
Q		146.15	0.00	0.00	
H	HIS	151.9	0.00	0.00	
G	GLY	75.07	28.27	219.97	220
T	THR	119.12	0.00	0.00	
R	ARG	174.2	0.00	0.00	
A	ALA	89.1	0.80	5.17	3
Y	TYR	181.19	0.00	0.00	
C	CYS	240	0.00	0.00	
V	VAL	117.15	29.60	145.53	150
M	MET	149.21	0.00	0.00	
W	TRP	204.33	0.00	0.00	
F	PHE	165.19	0.00	0.00	
I	ILE	131.18	14.07	61.75	60
L	LEU	131.18	1.57	6.90	6
K	LYS	146.65	0.71	2.90	3
P	PRO	115.13	21.38	108.43	110
			100,00	564,77	565

**B**

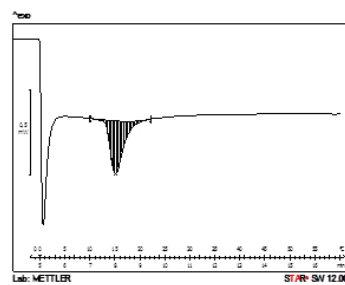
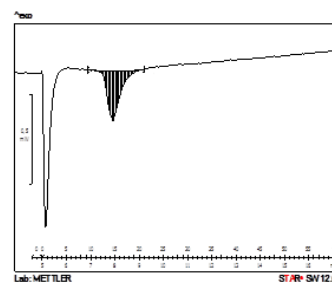
**Figure S2.** Characterization of control polymer. A: The amino acid composition was verified by high performance liquid chromatography (HPLC). B: The molecular weight of the recombinamer was determined by mass spectrometry (MALDI-TOF/MS).

**A**

	AA	Mr patron	Experimental		Theoretical
			% masa	count	count
D	ASP	133,11	2,04	3,24	3
E	GLU + GLN	147,13	3,92	15,35	16
N	ASN	132,12	0,00	0,00	
S	SER	105,09	0,00	0,00	
Q		146,15	0,00	0,00	
H	HIS	151,9	0,80	5,39	6
G	GLY	75,07	28,21	253,28	252
T	THR	119,12	0,74	1,25	1
R	ARG	174,2	1,31	2,11	2
A	ALA	89,1	2,11	6,17	7
Y	TYR	181,19	1,23	3,63	3
C	CYS	240	0,00	0,00	
V	VAL	117,15	26,41	152,72	157
M	MET	149,21	0,39		
W	TRP	204,33	0,75	3,53	4
F	PHE	165,19	0,93	3,84	3
I	ILE	131,18	11,24	65,12	63
L	LEU	131,18	2,71	10,23	9
K	LYS	146,65	0,63	2,97	3
P	PRO	115,13	16,59	110,47	111
			100,00	639,3	640

**B**

**Figure S3.** Characterization of Akt-in polymer. A: The amino acid composition was verified by high performance liquid chromatography (HPLC). B: The molecular weight of the recombinamer was determined by mass spectrometry (MALDI-TOF/MS).

**A****B**

**Figure S4.** Characterization of ELR polymers. Determination of transition temperature ( $T_t$ ) by differential scanning calorimetry (DSC) in PBS (pH 7.4). A: Control polymer. B: Akt-in polymer.

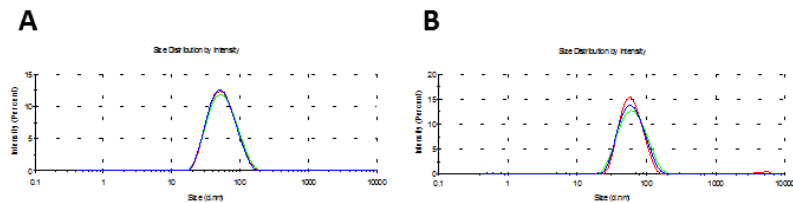


**Figure S5.** Characterization of ELR nanoparticles. Determination of size by dynamic light scattering in PBS buffer (pH 7.4) at 37°C at 0.5 mg/mL. A: Control polymer. B: Akt-in polymer.

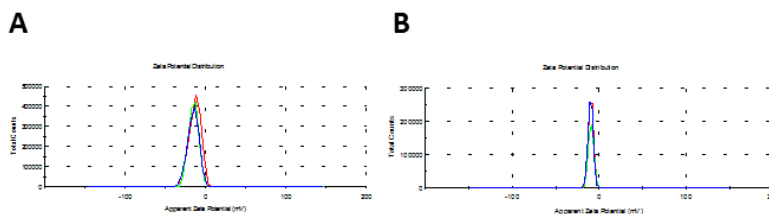


**Figure S6.** Characterization of ELR nanoparticles. Determination of z-potential measured by dynamic light scattering in ultrapure water type I at 37°C at 1 mg/mL. A: Control polymer. B: Akt-in polymer.

Nanoparticle	Time (h)	Size (nm)	PdI	Zeta Potential (mV)
Control NP	0	65.60 ± 3.73	0.087	-27.8 ± 1.5
	1	65.85 ± 3.23	0.070	-26.6 ± 1.4
	2	67.01 ± 2.78	0.134	-28 ± 1.8
	3	66.78 ± 2.46	0.127	-26.6 ± 1.2
Akt-in NP	0	72.46 ± 3.52	0.079	-26.2 ± 1.2
	1	73.2 ± 2.88	0.141	-25.8 ± 1.4
	2	72.08 ± 3.02	0.116	-25.4 ± 1.9
	3	71.71 ± 3.38	0.102	-25.9 ± 1.6

**Table S2.** Characterization of ELR nanoparticles. Size and polydispersity index of self-assembled polymers incubated with 5% BSA at 37°C measured by dynamic light scattering (DLS). Surface charge of self-assembled polymers measured by dynamic light scattering (DLS). Mean ± SD.

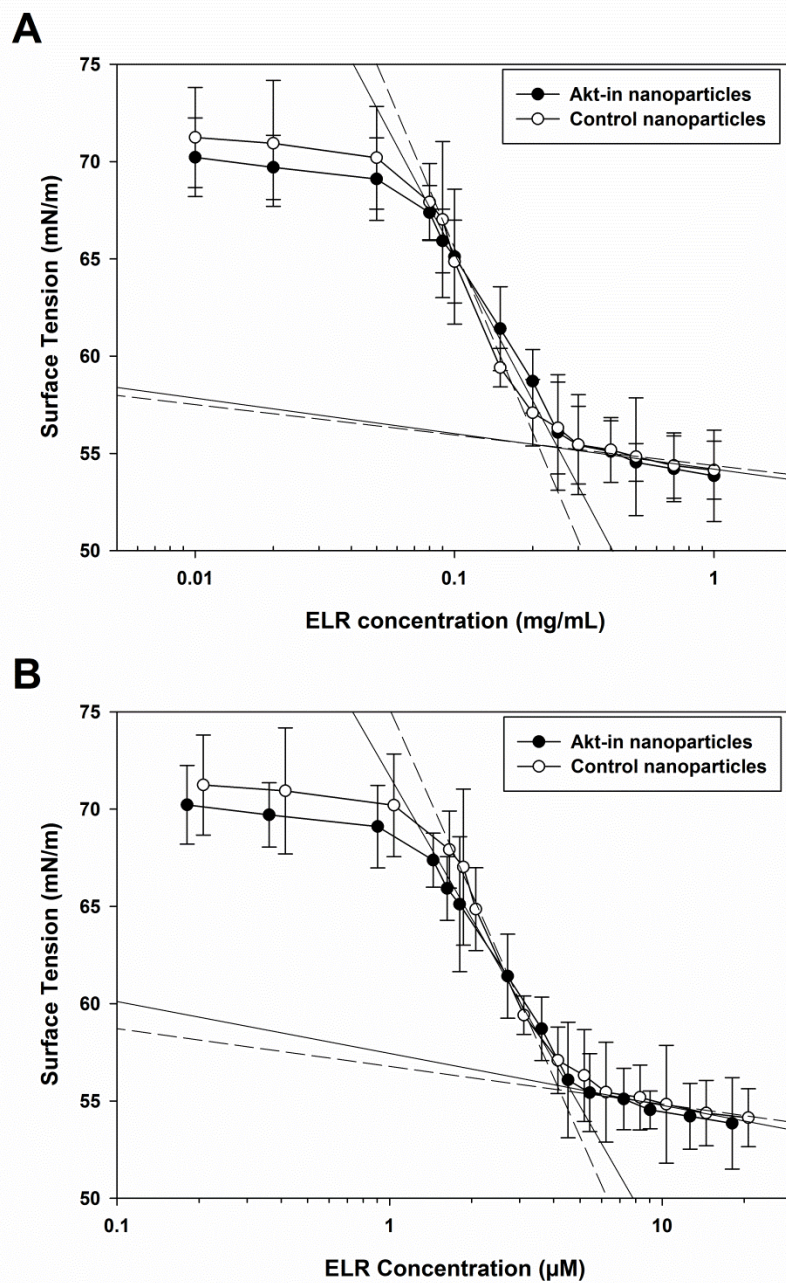


**Figure S7.** Characterization of ELR nanoparticles. Determination of critical micellar concentration (CMC) using the pendant drop method in PBS buffer (pH 7.4).

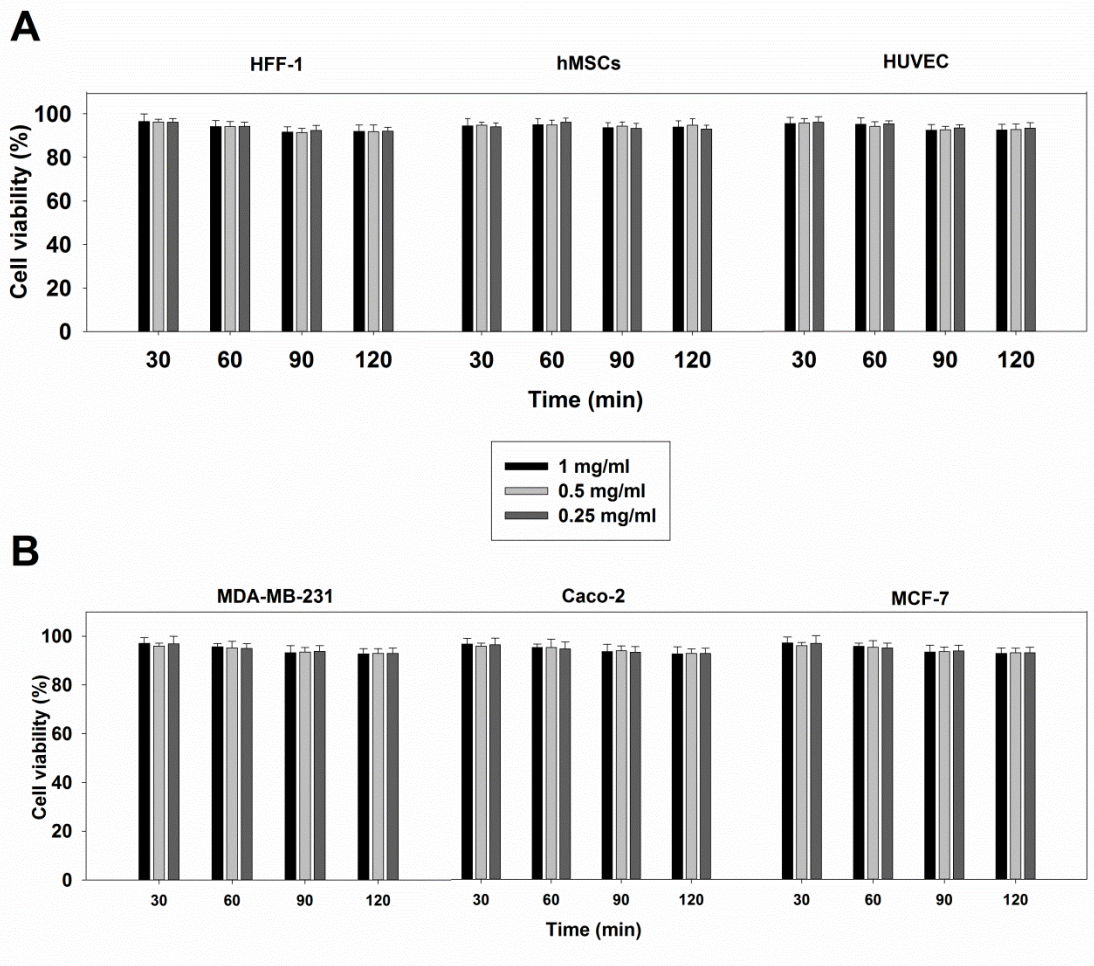


**Figure S8.** Percentage viability for HFF-1, hMSCs and HUVEC (panel A) and MDA-MB-231, Caco-2 and MCF-7 (panel B) with respect to untreated cells. Cells were incubated with control nanoparticles at three concentrations and times and viability was measured using the LIVE/DEAD kit Assay. n = 3 independent experiments, mean ± SD.